BIOMIMETIC IMAGING OF FLOW PHENOMENA

Saunvit Pandya[1], Yingchen Yang[1], Chang Liu[1], Douglas L. Jones[2]

[1]Micro and Nanotechnology Laboratory, University of Illinois at Urbana-Champaign
[2]Coordinated Sciences Laboratory, University of Illinois at Urbana-Champaign

ABSTRACT

Biologists have reported that fish form sensory maps to assist in the imaging of flow disturbances underwater, including those created by predator or prey, using the lateral-line flow-sensing system. Our group has invented artificial lateral-line systems based on both micromachined and commercial hot-wire anemometer sensors. In this paper, we report on the successful application of adaptive beamforming (Capon's method), in conjunction with an artificial lateral line, to visualize flow disturbances, including acoustic dipoles, underwater. Our preliminary results showcase, for the first time, an ability to image an entire region underwater using micro and millimeter scale arrays, thereby mimicking the flow-imaging abilities of fish.

Index Terms— Fluid flow measurement, underwater acoustic transducers, fluids, array signal processing, dipole arrays, anemometers, adaptive beamforming.

1. BACKGROUND

Researchers in the field of underwater biological sensing systems have long been aware of the importance of the lateral line organ found in many kinds of fish. The seminal work in this area, [1], highlighted the function of the lateral line, while [2] showed that fish can school using the lateral line system alone. Furthermore, biologists have discovered the ability of fish to form hydrodynamic maps [3] as well as the ability of fish to localize and track an acoustic dipole source [4]. Researchers have also characterized the signals that a lateral line would receive from a hydrodynamic stimulus [5].

Our work has been to develop a system-level engineering imitation of the biological lateral line for use on unmanned underwater vehicles (UUVs), intrusion detection systems (IDs), hydro-robotics, and other defense systems. The "distant touch" imaging sense that the lateral line provides for biological creatures would be invaluable for navigation, targeting, position maintenance (rheotaxis), and especially, close-in maneuvering. Developing an artificial lateral-line system necessitates the development of both biomimetic "hardware" as well as biomimetic "software"

components. The biomimetic "hardware" developed by our group consists of a portfolio of high-sensitivity, high-density (arrayed), micromachined sensors including hot-wire anemometers [6] and haircell sensors. Furthermore, our group has invented approaches to use arrays of commercial, millimeter-scale hot-wire anemometers as a millimeter-scale lateral-line equivalent. In this paper, we focus on the use of the commercial, millimeter-scale hot-wire anemometers, since these sensors are easily obtainable by those who wish to replicate our experiments.

A complete artificial lateral line requires a suite of signal-processing algorithms to accompany either microsensor or commercial sensor arrays. Previous work in this area primarily consists of microsensor-based algorithms developed for localizing and tracking an acoustic dipole source [7] using ML estimators and techniques. Adding an ability to image flow regions as well as respond to imprecise stimuli (flow disturbances rather than pure acoustic dipoles) would greatly improve the capability of an artificial lateral-line system as well as improve the system's fidelity to the biological models.

2. EXPERIMENTAL DESIGN

An enclosed water channel with near-stationary flow was used as a testing environment (Figure 1). A dipole source (a small sphere mounted longitudinally to the axis of a shaker/oscillator) was oscillated at frequencies of 40 and 75 Hz at different points around a sensor array.

The sensor array, itself, was tested in two geometries. The first geometry consisted of 16 HWAs arranged in a linear configuration (Figure 1a). The second geometry consisted of 13 HWAs in an airfoil geometry around a solid inner airfoil, thereby mimicking the shape of a fish (Figure 1b and 1c). This geometry is henceforth referred to as the "artificial fish." However, we decided to remove the inner airfoil, in order to decouple flow phenomena from the fish body. This would, in effect, make the artificial fish "transparent."
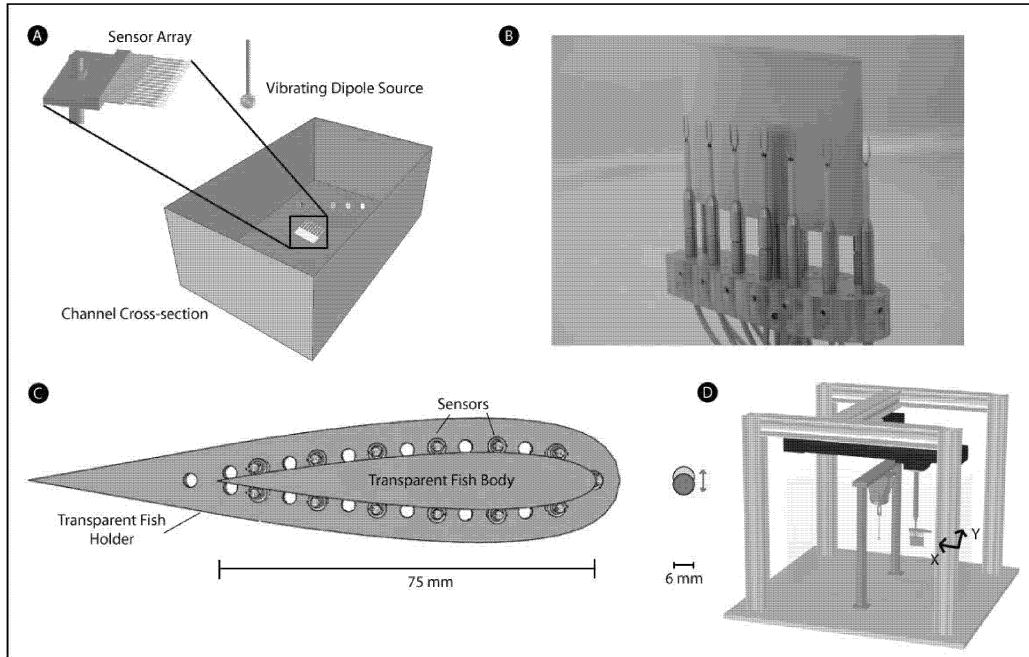
Figure 1: *A)* Illustration of a linear array of commercial HWA sensors in the testing facility along with an example dipole progression. *B)* A picture of the artificial fish with the inner airfoil. *C)* Schematic drawing of the artificial fish from the bottom view. *D)* Schematic of testing facility with dimensional axes indicated.

The initial position of each array was measured with respect to the dimensions of the tank (Figure 1d). As mentioned before, the dipole was oscillated at various positions relative to each array. The coordinates of the dipole positions were recorded from a Newport stage-control system, on which the entire shaker-dipole apparatus was mounted. This system, accurate to within several micrometers, allowed us to record the relative position of the dipole and the fish in two dimensions with also a precise, angular measure to track successive dipole movements.

For the linear array, 31 positions relative to the array were mapped at a dipole oscillation frequency of 75 Hz. For the artificial fish, 10 positions relative to the array were mapped at each dipole oscillation frequency (40 and 75 Hz). Furthermore, several additional measurements were taken for the artificial fish, in which an imprecise flow-acoustic disturbance was used as a stimulus.

Signals from a specific geometry at an experimental point were collected by an instrumentation and measurement system (NI DAQ), using the software Labview. These signals were then sampled at a rate of 2048 samples/second, in order to assure sampling at a rate significantly higher than the Nyquist frequency. Two seconds of data were collected at each empirical data point.

As mentioned previously, the coordinates of both the array and the dipole were taken relative to each other and to the dimensions of the testing facility. For algorithm purposes, locations in the water channel were mapped onto a grid. Two approaches were taken corresponding to the two array geometries. In each approach, an endpoint of a particular array geometry was taken as the grid origin.

3. ALGORITHM

The first step in the algorithm was to create a template $s_{x,y}$ for each point (x,y) in the grid by computing the expected sensor readings from an analytical model for a dipole located at (x,y). The location of the sensor array, for the linear geometry, was from the origin to $(d(n-1), 0)$, where n represents the number of sensors and d the spacing between each sensor. For the artificial fish, the location of the sensors on the grid was mapped using the same equation that governed the design and manufacturing of the inner airfoil. The form of a template for the linear geometry is shown in Eqn. 1.

$$\mathbf{s} = [s_1 \, s_2 ... s_{16}]^T \qquad (1)$$

The analytical model (Eqn. 2) is similar to the ones found in [7-9], but was normalized to take the magnitude of the overall dipole flow field rather than the magnitude in any one direction. This is partially due to the fact that the HWA sensor measures flow magnitude not flow direction.
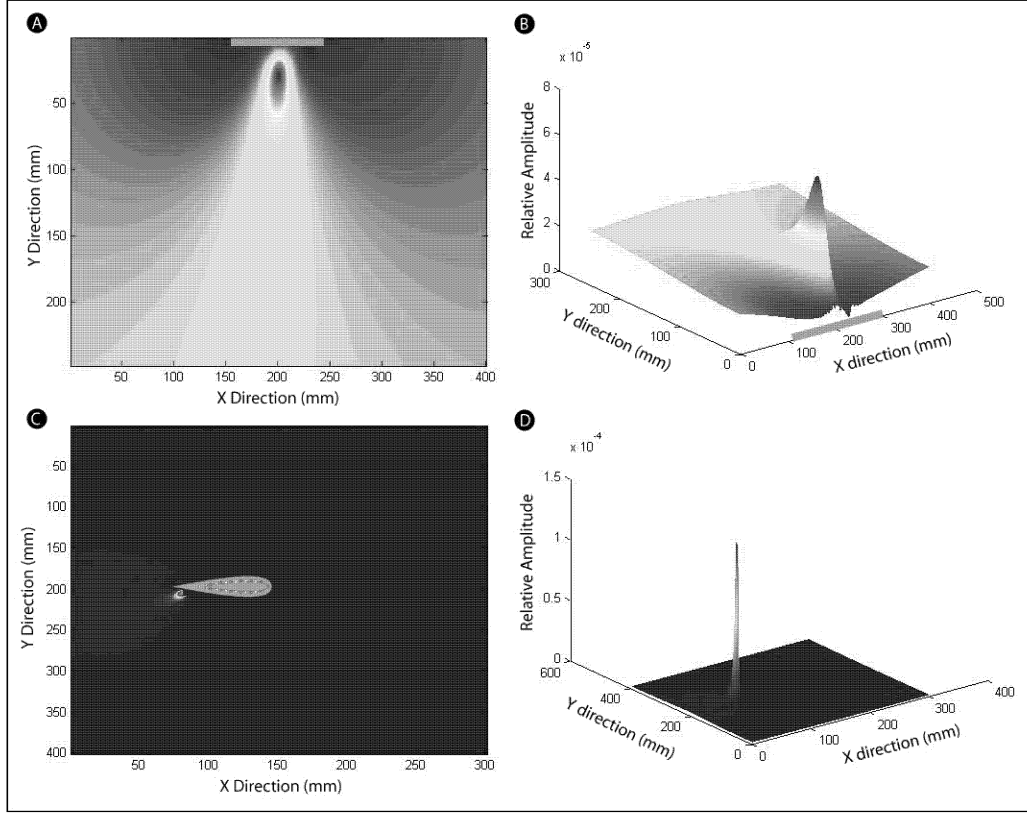
Figure 2: *A)* 2D representation of a linear array successfully imaging an oscillating dipole source (in-scale location of array is indicated by a brown box). *B)* 3D representation of the energy distribution. *C)* 2D representation of artificial fish array successfully imaging an oscillating dipole source. *D)* 3D representation of the energy distribution around the artificial fish.

$$V = \frac{V_o a^3}{2r^3} \qquad (2)$$

In the above equation, V represents the fluid velocity at that point, V_o represents the initial vibrational velocity, a represents the diameter of the vibrating sphere (dipole source), and r represents the distance between a grid point (x,y) and the corresponding sensor coordinates. V_o was in turn computed by multiplying the dipole frequency (in rad/s) by the vibrational amplitude X_o (Eqn. 3).

$$V_o = 2\pi f X_o \qquad (3)$$

After this step was completed, a template database was compiled featuring n sensor readings (dependent on the geometry) for each point (x,y) in the grid.

Following this, a running outer-product (Eqn. 4) was computed over all the samples and channels (sensors) for each data point to obtain an empirical estimate of the correlation matrix. In Eqn. 4, **R** is the outer-product, whereas **x**[n] refers to the discrete-time vector of samples of the collected data.

$$\mathbf{R} = \frac{1}{N} \sum_{n=1}^{N} \mathbf{x}[n] \cdot \mathbf{x}[n]^T \qquad (4)$$

Our goal is to obtain a high-resolution map of the position of the dipole sources around the array. [8] has proposed the use of a continuous wavelet transform (CWT) for use on data from linear geometries. However, this method is adequate for only linear geometries, and offers poor resolution.

We instead propose an adaptive beamforming approach using Capon's method [10]. Eqn. 5 was used to compute the energy level at each point in the grid, with **R** being the empirical correlation computed above and **s** being a generalized steering vector for the target at a grid point (x,y).

$$E = \frac{1}{\mathbf{s}^H \mathbf{R}^{-1} \mathbf{s}} \qquad (5)$$

Once computed, the energy level was subsequently plotted, and thus yielded the location of the acoustic dipoles and/or flow disturbances. The energy level at each point

was furthermore used to image a region. A regularization factor was added to the outer-product in order to make the beamforming method more robust to deviations from the assumed signatures [11].

4. RESULTS AND CONCLUSIONS

Results from several test cases are summarized in Figure 2. Figures 2a and 2b show the successful imaging of a dipole source as the source diagonally traverses the linear array. The particular imaging point, shown in Figures 2a and 2b, is taken when the source is approximately at the midpoint of the array. The imaging error is less than 10%. As the dipole moves away from the array, the target resolution becomes poorer due to the inherent broadening of the dipole response across the array. Figure 2a shows the 2-dimensional location in the grid, whereas 2b shows the energy level for the entire grid region.

Figures 2c and 2d show similar results for the artificial fish geometry. In this case, the dipole was slightly off the tail end of the artificial fish. The imaging in this case is believed to be within 5%. Various degrees of success in imaging were seen in the range of 20-80 mm. on any side of the fish. However, due to the transparent nature of the artificial fish, ghost images often resulted when a dipole was placed on the side of the fish. We believe that a solid fish-body (using the inner airfoil) will lead to a significant increase in imaging performance with the artificial fish as long as the interference effects of the fish body are properly configured into the analytical signature.

Furthermore, using the artificial fish, we were able to detect a "flow anomaly" created by a human finger (Figure 3). Although this anomaly created ghosts on the image (which were similar to ghosts often seen when the dipole source was placed alongside the array), we believe that future refinements in the algorithm will allow us to detect more general dipole-like sources. The anomaly's actual location is currently off by 15-20% from the location given by the imaging algorithm.
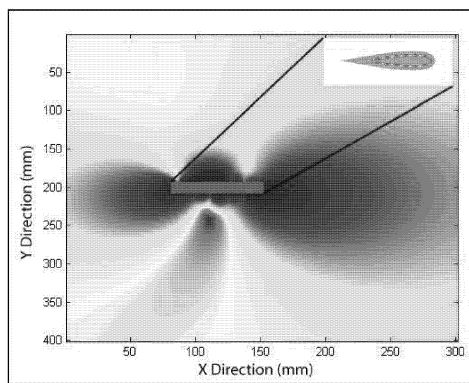

Figure 3: Successful imaging of a flow anomaly.

6. REFERENCES

[1]   S. Dijkgraaf, "The functioning and significance of lateral-line organs.," *Biol. Rev.*, vol. 38, pp. 51-105, 1963.

[2]   T. Pitcher, B. Patridge, and C. Wardle, "A blind fish can school.," *Science*, vol. 194, pp. 963-965, 1976.

[3]   S. Coombs, J. J. Finneran, and R. A. Conley, "Hydrodynamic image formation by the peripheral lateral line system of the Lake Michigan mottled sculpin, Cottus bairdi," *Philosophical Transactions of the Royal Society B: Biological Sciences*, vol. 355, pp. 1111-1114, 2000.

[4]   S. Coombs and R. A. Conley, "Dipole source localization by mottled sculpin. I. Approach strategies," *Journal of Comparative Physiology A: Neuroethology, Sensory, Neural, and Behavioral Physiology*, vol. 180, pp. 387-399, 1997.

[5]   J. Engelmann, W. Hanke, J. Mogdans, and H. Bleckmann, "Hydrodynamic stimuli and the fish lateral line.," *Nature*, vol. 408, pp. 51-52, 2000.

[6]   J. Chen, J. Engel, N. Chen, S. Pandya, S. Coombs, and C. Liu, "Artificial Lateral Line and Hydrodynamic Object Tracking," presented at The 19th IEEE International Conference on Micro Electro Mechanical Systems, Istanbul, Turkey, 2006.

[7]   S. Pandya, Y. Yang, D. L. Jones, J. Engel, and C. Liu, "Multisensor Processing Algorithms for Underwater Dipole Localization and Tracking Using MEMS Artificial Lateral-Line Sensors," *EURASIP Journal on Applied Signal Processing*, pp. In Press, 2006.

[8]   B. Curcic-Blake and S. M. v. Netten, "Source location encoding in the fish lateral line canal," *The Journal of Experimental Biology*, vol. 209, pp. 1548-1559, 2006.

[9]   S. Coombs, "Dipole3D User Guide," Loyola University, Chicago, IL 2003.

[10]   J. Capon, "High-resolution frequency-wavenumber spectrum analysis," *Proceedings of the IEEE*, vol. 57, pp. 1408-1418, 1969.

[11]   H. Cox, R. M. Zeskind, and M. M. Owen, "Robust Adaptive Beamforming," *IEEE Transactions on Acoustics, Speech, and Signal Processing*, vol. 35, pp. 1365-1376, 1987.